# Thermal Imaging for Assessment of Electron-Beam Free Form Fabrication ($EBF^3$) Additive Manufacturing Welds

Joseph N. Zalameda*[a], Eric R. Burke[a], Robert A. Hafley[a], Karen M-B. Taminger[a], Christopher S. Domack[b], Amy Brewer[c] and Richard E. Martin[a]

[a]NASA Langley Research Center Hampton, VA 23681-2199;
[b]Analytical Mechanics Association; [c]Northrup Grumman; NASA Langley Research Center Hampton, VA 23681-2199

## ABSTRACT

Additive manufacturing is a rapidly growing field where 3-dimensional parts can be produced layer by layer. NASA's electron beam free-form fabrication ($EBF^3$) technology is being evaluated to manufacture metallic parts in a space environment. The benefits of $EBF^3$ technology are weight savings to support space missions, rapid prototyping in a zero gravity environment, and improved vehicle readiness. The $EBF^3$ system is composed of 3 main components: electron beam gun, multi-axis position system, and metallic wire feeder. The electron beam is used to melt the wire and the multi-axis positioning system is used to build the part layer by layer. To insure a quality weld, a near infrared (NIR) camera is used to image the melt pool and solidification areas. This paper describes the calibration and application of a NIR camera for temperature measurement. In addition, image processing techniques are presented for weld assessment metrics.

**Keywords:** E-beam welding, additive manufacturing, near infrared (NIR) imaging, image analysis, melt pool, nondestructive evaluation

## 1. INTRODUCTION

Three-dimensional printing or additive manufacturing is a "game changing" technology and is a rapidly growing field where parts can be produced layer by layer. This technology is expected to have a significant impact in many areas including industrial manufacturing, medical, architecture, aerospace, and automotive. NASA's electron beam free form fabrication ($EBF^3$) technology is being evaluated to manufacture metallic parts, using layer by layer metal deposition, for both aerospace and space applications [1-3]. The advantages of additive manufacturing are reduction in material costs due to near net shape part builds, minimal machining required, computer assisted builds for rapid prototyping, and mass production capability. For space applications, the benefits of $EBF^3$ technology are weight savings to support space missions, rapid prototyping in a zero gravity environment, and repair for improved vehicle readiness.

The NASA $EBF^3$ system is composed of 3 main components: electron beam gun, multi-axis positioning system, and metallic wire feeder. Using wire in space is preferred to metal powders due to dispersion in a zero gravity environment. A picture of the setup is shown in Figures 1a and 1b. The entire system is contained in a vacuum chamber, Figure 1a, to minimize contamination. The overall size of the chamber is 2.13 x 2.74 x 2.74 meters. The electron beam is used to melt the wire and the voltage is typically around 30 KV with beam currents of 10 – 100 milliamps. The beam can be focused and controlled for scanning in various patterns such as raster or circular. The beam can also be defocused to heat a relatively large area. Typical focused beam size is approximately 0.04 cm in diameter. The multi-axis positioning system controls the build, layer by layer, in the X, Y, Z, and rotational directions. The metallic wire is fed using a rotating spool that is remotely controlled and this allows for adjustment in wire feed rate. The typical diameter of a stainless steel wire is approximately 0.165 cm in diameter.

The operation of the $EBF^3$ system requires a baseplate which serves two main purposes. First as the platform to build the part and secondly it acts as a heat sink to conduct heat away from the welding process. The baseplate is clamped to a mounting fixture to minimize warping due to welding induced distortions.

*joseph.n.zalameda@nasa.gov; phone 1 757-864-4793; fax 1 757-864-4914; http://nde.larc.nasa.gov/majorcap.shtml

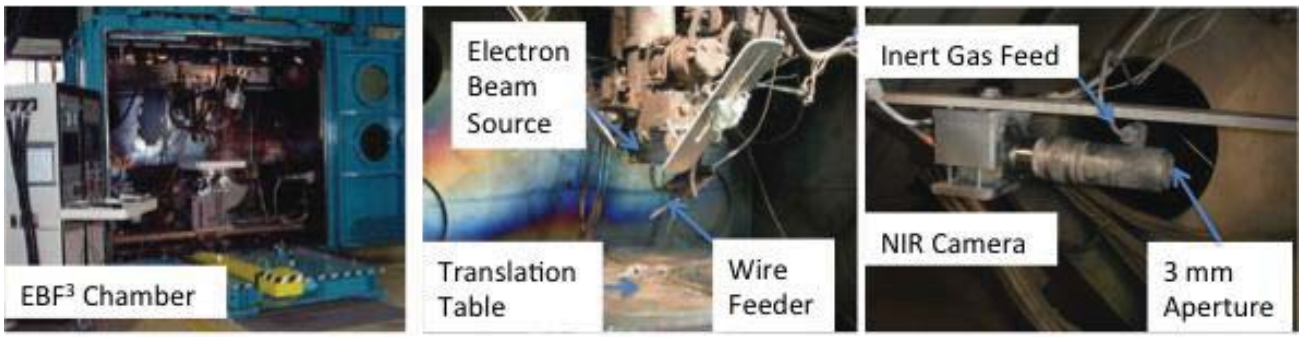


Figure 1. EBF$^3$ chamber and main components.

Before a weld bead is placed on the baseplate, a heating pass is performed to clean the area and remove any oxide layers. The part can then be built layer by layer using the electron beam to melt the wire as the baseplate is moved. Parameters, such as positioning speed, wire feed rate, wire Z height from the melt pool, beam power, and beam focus are critical for controlling the quality of the build. To observe the welding process, a near infrared (NIR) camera is used to image the melt pool and solidification areas. This paper describes the calibration and application of a NIR camera for temperature measurement. In addition, image analysis techniques are presented for weld assessment.

## 2. NEAR INFRARED (NIR) CAMERA SYSTEM

### 2.1 NIR Camera

The digital NIR camera used is the Prosilica GC1380H and is shown in Figure 1c. This is a non-cooled camera. The camera pixel array size is 1360x1024 with a frame rate of 30 Hz at full resolution through a GigE interface. The camera's dynamic range is 12 bits. This wide dynamic range is valuable in minimizing image saturation. The integration time can be varied from 10 μsec. to 60 sec. in real time. The spectral response of the camera's CCD sensor is 0.4 – 1.05 μm [4]. A long pass filter with cut on at 0.900 μm is used to remove the spectral energy in the visible band. A NIR neutral density filter is used to reduce the transmission by a factor of 10. This was necessary to minimize saturation and allow for integration time adjustments over a wider range from 100 – 1500 μsec. In addition to the long pass filter and neutral density filter, the C-mount optical package contains a 150 mm relay lens pair, a protective window (B270 material), and an extension tube with a gas fitting. The gas fitting allows for a small amount of inert gas to flow out of the 3 mm diameter aperture and thus prevent window clouding due to residual metallic particles dispersed during the electron beam excitation. The NIR camera is located in line with the weld bead opposite the wire feeder and is positioned approximately 60 degrees to the weld pool. Camera resolution is approximately 0.006 cm/pixel.

### 2.2 NIR Camera Radiometric Calibration

The radiometric characterization was performed using a calibrated blackbody radiation source set at various temperatures [5-7]. The calibration setup is shown in Figure 2. The process involves the calibration of the radiance counts to actual temperature values. The calibration was performed at temperatures of 700, 800, 900, 1,000 and 1,100 degrees Celsius at specified sensor integration times of 200, 500, 1,000, 5,000, 10,000, 20,000 and 50,000 μsec. The sensor response is shown in Figure 3(a). The pixel intensity counts were determined by averaging 100 pixels within the center of the imaged blackbody. The averaged error was approximately +/- 9 counts for all the points shown. In order to determine the correct radiance values, the overall spectral response of the imaging system must be defined. This is determined by combining the spectral response of the long pass filter, the neutral density filter, and the CCD's quantum efficiency spectral curve. From this the spectral band of interest was determined to be from 875 to 1050 nm.

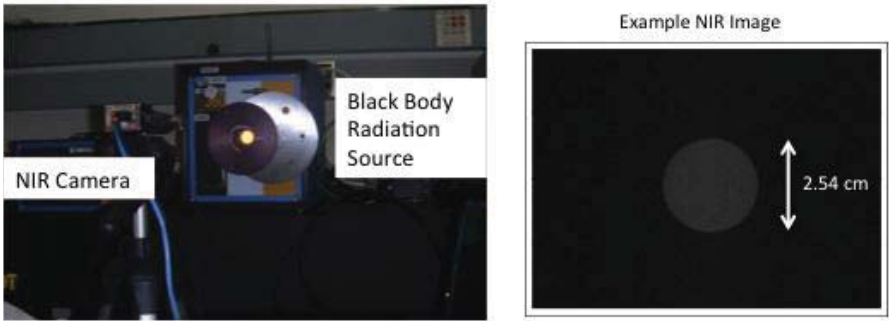


Figure 2. Direct view calibration.

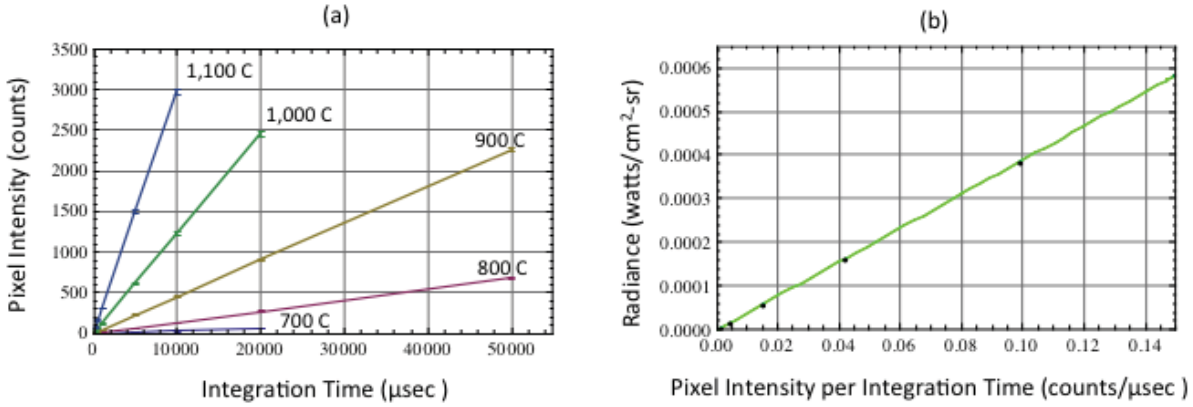


Figure 3. Calibration results.

Using the overall system's spectral response, Planck's equation is then numerically integrated over this spectral band for a range of temperatures (500 – 2500 degrees Celsius) to provide the system's radiance response. Using the blackbody calibration data, the measured pixel intensity can then be related to the in-band radiance for a given temperature. This is shown in Figure 3(b) where the pixel intensity counts per integration time is linear to radiance (watts/cm$^2$-sec). The correlation coefficient (r-squared) value is 0.999987 for Figure 3(b). For a given integration time and measured counts, the in-band radiance can then be determined. Using the correct emissivity value, the radiance is then converted to temperature using a linear interpolation of the system's radiance response. Example temperature images are shown in Figures 4 and 5 for Ti 6-4 and 316 stainless steel respectively. The weld beads are approximately 0.32 cm wide.

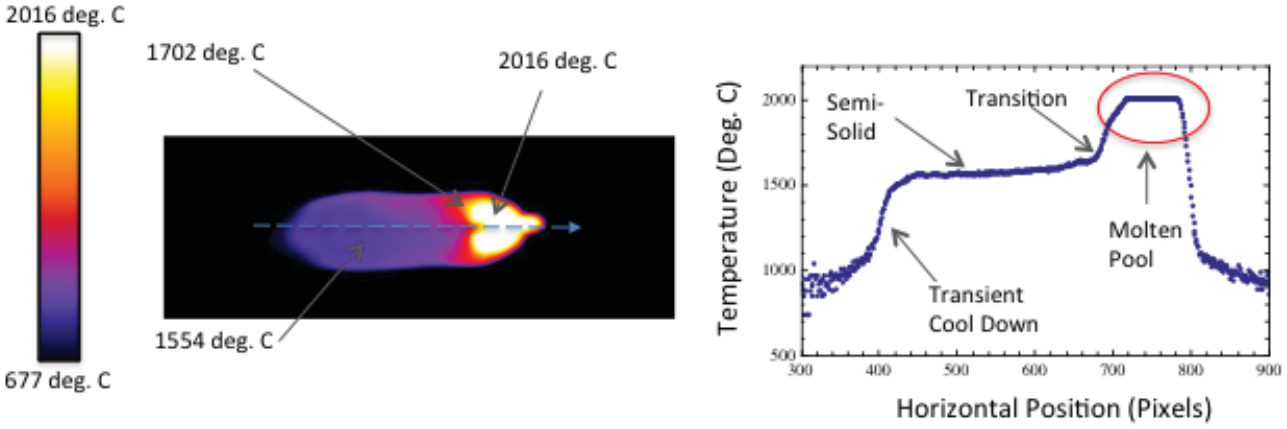


Figure 4. Example image results on Ti6-4 with temperature line plot.

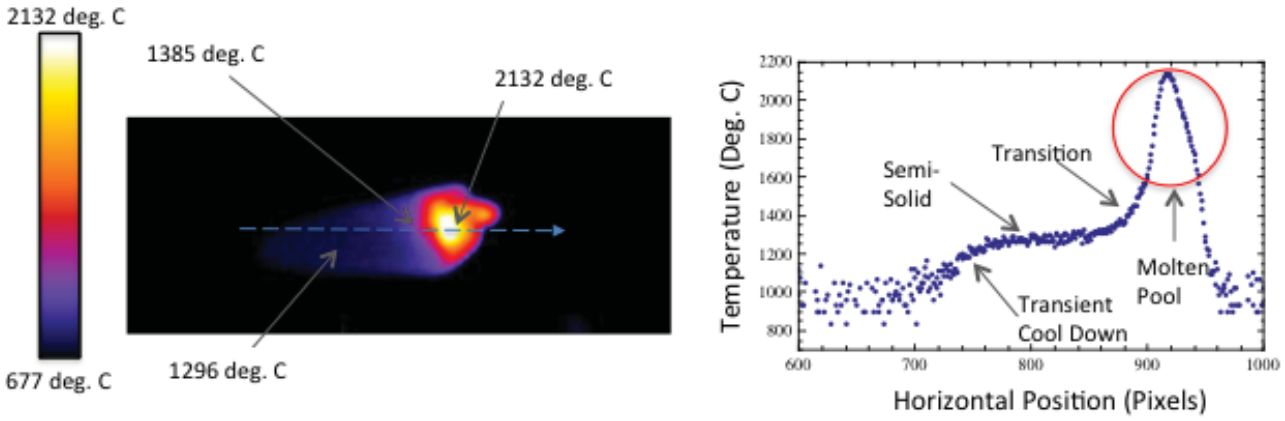


Figure 5. Example image results on 316 stainless steel with temperature line plot.

The camera integration times and frame rate were 1,000 µs at 30 Hz for the Ti6-4 measurements and was 200 µs at 30Hz for the stainless steel. The emissivity values used for 316 stainless steel and Ti6-4 were 0.66 and 0.48 respectively [10,11] and averaged values were used over the temperature range of interest. As shown the measured temperature values show good agreement to literature values [8,9] at the transition points for the respective melting points (1,385 deg. C for 316 stainless steel and 1,632 deg. C for Ti6-4). The camera calibration is critical for setting the proper threshold values for closed loop control feedback efforts discussed later in this paper.

## 3. IMAGING DURING WELDING FABRICATION

Using the NIR camera, real time images of the additive welding process are obtained. The camera is positioned opposite the wire feeder so that the weld pool and semi-solid area is not blocked by the wire feeder during a positive X direction deposit. The camera output can be used to provide real time feedback to the weld operator. This can be particularly important if the viewing window clouds up due to dispersed metal produced by the electron beam. An automated or closed loop control (CLC) feedback system can be more desirable to control welding parameters [12-14]. The weld parameters such as beam power, wire feed rate, wire feed height, and translation speed can be automatically adjusted. A CLC system would require image metrics to be obtained during the free form build process. In addition the image metrics could provide valuable information about the quality of the weld.

### 3.1 Data Processing for Weld Metrics

An example image of a 316 stainless steel circular deposit is shown in Figure 6. From this image weld metrics such as saturated pixels, average pixel intensity, melt pool area and tail area can be obtained. The melt pool area is determined by summing the pixels with intensities between 595 to 4095 counts. The 595 counts value corresponds to 1,385 deg. C and is determined from the calibration for an integration time of 1,000 µs. The image acquisition frame rate was 3 Hz.

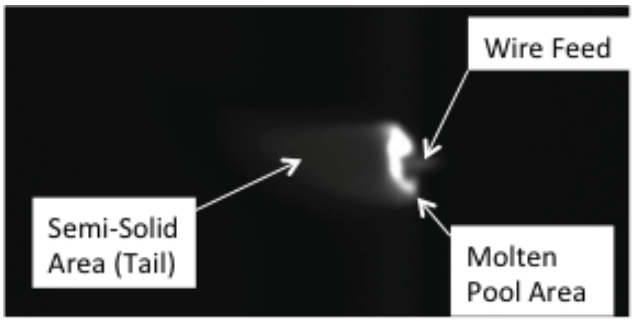


Figure 6. Example image of 316 stainless steel deposit.

The melting point of 316 stainless steel range is 1,370 to 1,400 deg. C. and 1,385 is the middle of that range [8]. The emissivity value of 0.66 was used for stainless steel [10]. Count values higher than 595 corresponds to super heated melted steel. The tail length values were determined using values of 237 – 594 counts that relate to 1,221 to 1,384 deg C. These values provide the range of steel solidification initiation to complete solidification. At complete solidification the transient cool down occurs. The number of saturated pixels per image and the averaged intensity counts is plotted in Figure 7a and 7b respectively. The total build time was approximately 11 minutes. The average intensity counts plot increases steadily due to the temperature rising during the continuous build. The saturated pixels number appears to vary randomly.

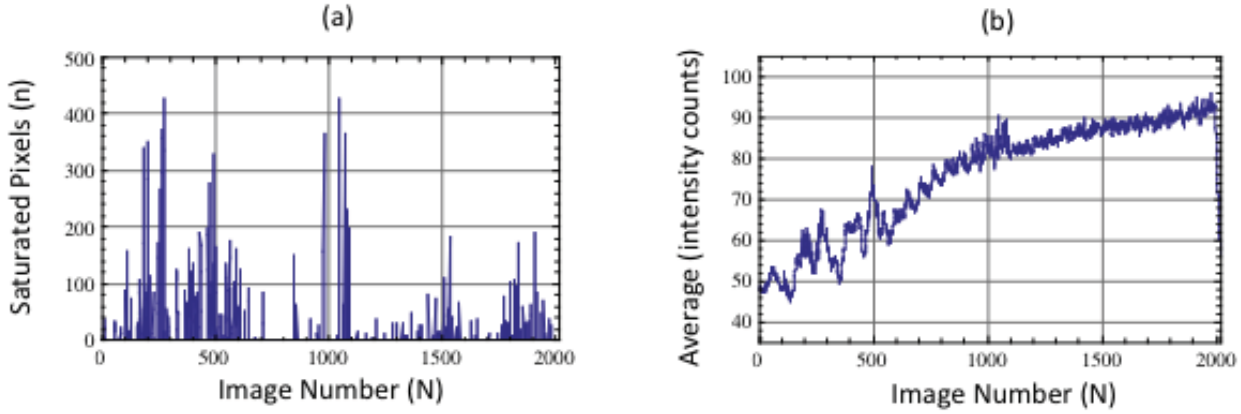


Figure 7. Image saturation and average intensity metrics during stainless steel build.

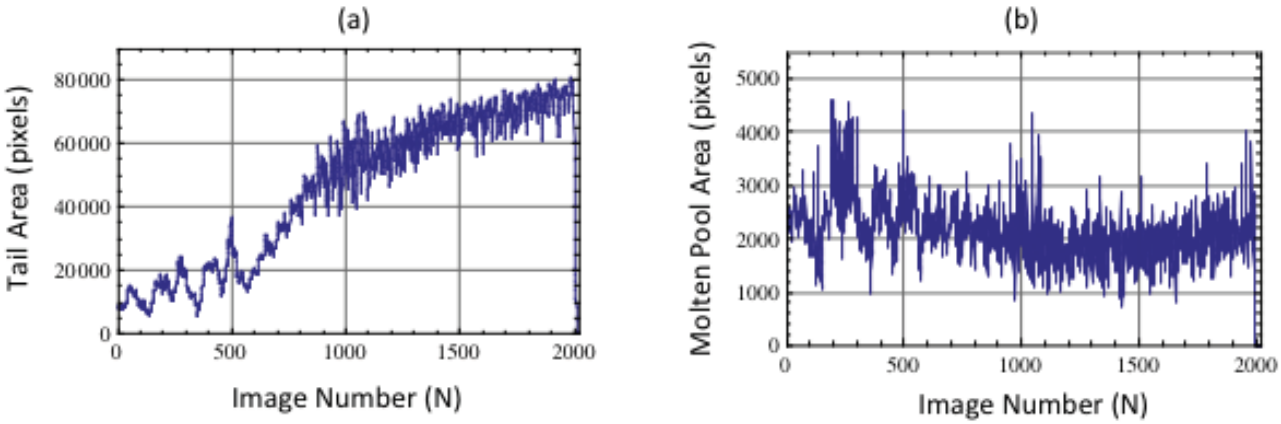


Figure 8. Image tail area and molten pool metrics during stainless steel build.

Similarly, the tail area size per image and the molten pool area pixel counts are plotted in Figure 8a and 8b respectively. The tail area grows over time during the continuous build. This is due to the temperature of the base plate rising resulting in a higher temperature offset and an increase in the amount of time it takes for the molten metal to solidify. The molten pool area varies over image number and is a good candidate for CLC since the molten pool is not sensitive to the offset temperature. The molten area size is sensitive to beam power. Based on these results, a CLC algorithm was developed to control the beam power based on measured molten pool area. If the molten pool area is kept fixed to a certain value then the beam power can be adjusted accordingly. The results of these efforts are shown in Figure 9 where 20 layer single wall 316 stainless steel builds are compared. The power and wire Z height are kept fixed during the application of the 20 layers for the no control build on the left. The power and Z height are manually controlled for the middle cross section build and the CLC single wall build (right image) is based on automatic adjustment of beam power based on a fixed molten pool area. A qualitative comparison reveals the manual control build is more uniform in cross

sectional area. The CLC build is comparable to the manual control build considering there was no wire Z height adjustment. It is expected that automatic wire Z height adjustment would improve the cross section uniformity of the CLC build. Therefore a second camera would allow for automating the wire Z height adjustment and thus provide another feedback parameter for CLC.

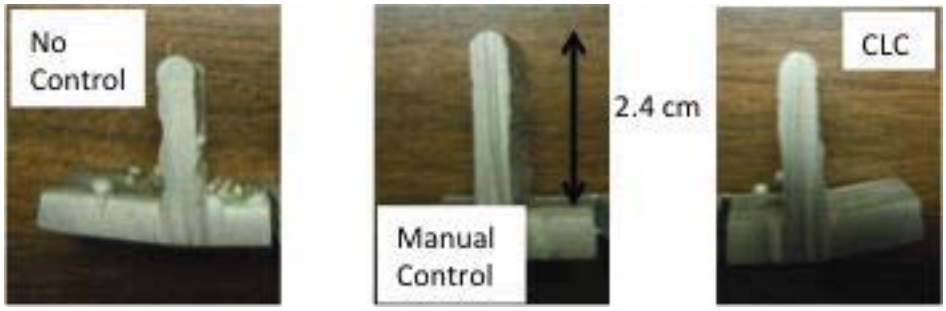


Figure 9. Cross section comparison of stainless steel single wall builds.

### 3.2 Weld Nondestructive Evaluation using Transient Cool Down

An interesting characteristic of the weld thermal response is the transient cool down after solidification. This transient response is typically used in thermal nondestructive evaluation where the decay in temperature is related to the thermal properties of the material and the thickness. Traditional thermal nondestructive evaluation (NDE) techniques typically use flash or quartz lamp heating to induce a temperature rise [15,16]. The defects such as a cracks, delamination damage, or voids would block the heat flow and therefore cause a change in the transient response. Also areas of material thickness variations could also be detected. In this case, the heat source is moving over the sample and allows for inspection over the area of the build. This is similar to other thermal NDE techniques using a moving heat source [17,18]. To test this, a baseplate sample was made with overall thickness of 0.64 cm. Defect areas with residual thicknesses of 0.254 cm with different rectangular size areas of 0.32 cm x 1.27 cm (A), 0.64 cm x 1.27 cm (B), and 1.27 cm x 1.27 cm (C) and with residual thickness of 0.476 cm and with areas of 0.32 cm x 1.27 cm (D), 0.64 cm x 1.27 cm (E), and 1.27 cm x 1.27 cm (F) were made. A single weld layer is approximately 0.185 cm so a residual thickness on that order would correspond to a disbond between successive build layers and greater thickness would correspond to defects under multiple layers. To test this, wire deposits were performed on the NDE sample over the defect areas. The results are shown in Figures 10 and 11. The NDE image is calculated by averaging the cool down transient intensity counts within a time window.

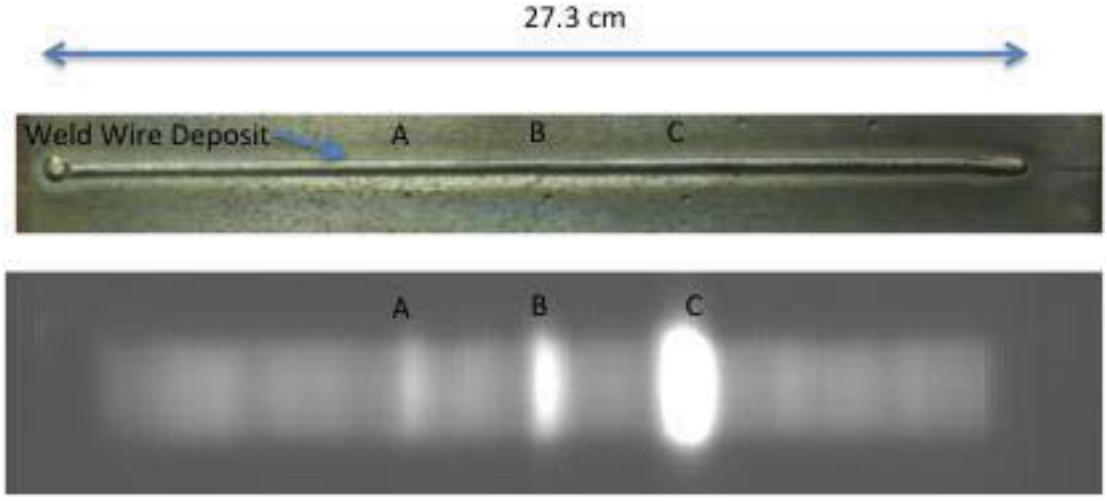


Figure 10. NDE image from single wire deposit weld.

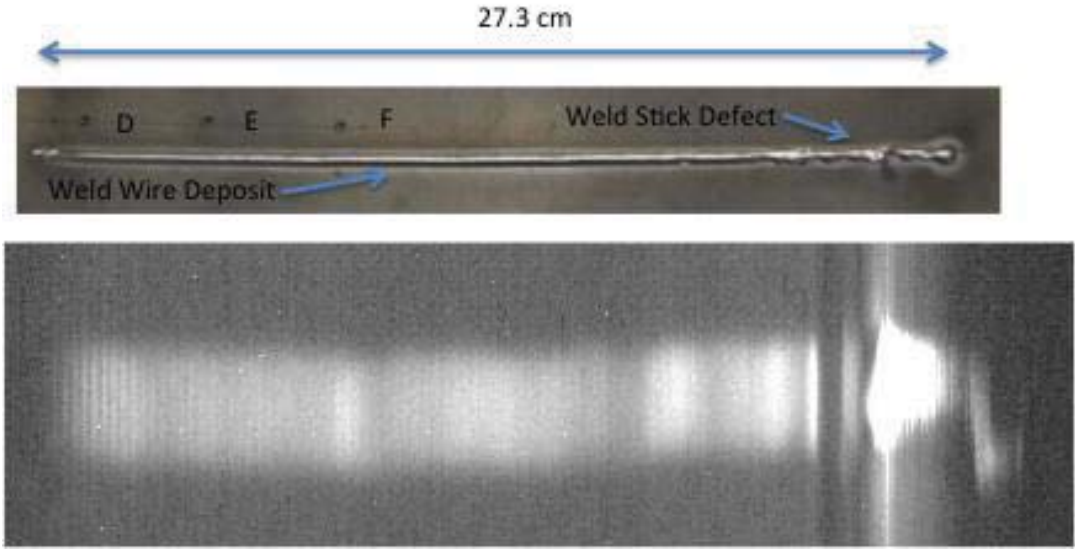


Figure 11. NDE image of wire deposit over deeper defects.

Since the sample is moving with respect to the camera during welding, the time window is a spatial section for each image. For the NDE image in Figure 10 the time window used was 3.3 seconds (30 Hz frame rate) starting at approximately 153 pixels from the center of the weld pool. The NDE image in Figure 10 is able to detect the thin areas within the baseplate under a deposited layer. The plate velocity was approximately 101.6 cm/sec. The NDE image in Figure 11 used a time window of 3.3 seconds starting at approximately 168 pixels from the center of the weld pool. This greater number of offset pixels allowed for a deeper inspection since the measurement must see past the deposited wire and into the base plate. Defects D, E, and F were not detected. This might be due to the residual thickness (.476 cm) being 75 percent of the baseplate thickness. This would be equivalent to looking through 3-4 deposited layers. A more sensitive infrared camera would allow for deeper inspections. The NDE image of Figure 11 does show variations in intensity during the deposition which can be attributed to non-uniform deposit and a weld defect (stuck wire) at the end.

## 4. CONCLUSIONS

A near infrared (NIR) camera was used to image the melt pool and solidification areas for the EBF$^3$ system. The NIR band was appropriate due to the high temperatures required for welding TI6-4 and 316 stainless steel. The calibration was confirmed by measuring the transition point between the molten/solidification areas for Ti6-4 and 316 stainless steel. The transition points for Ti6-4 and 316 stainless steel were approximately 1,632 deg. C and 1,385 deg. C respectively. This confirms that the molten areas are measured correctly. The calibration performed was essential for the measurement of weld pool area and solidification (tail) areas. These areas were used as metrics for the CLC efforts. By adjusting the beam power through the molten pool area, an improved weld was obtained compared to no control. Finally the transient section of the weld response curve was helpful for NDE of the weld, although more measurements are required. This allows the infrared camera to serve a dual purpose: first to be used as the CLC feedback sensor and secondly to document the quality of the weld through inspection during the fabrication process.

## 5. FUTURE DIRECTIONS

As discussed previously, additional camera viewing angles would improve the CLC. A camera on the side would help determine the wire Z height. Also if the direction of travel is in the negative X direction, the current camera view of the weld pool and tail areas would be blocked by the wire feeder. To address this, a dual camera configuration, viewing from opposite sides would allow imaging in all travel directions without the wire feeder blocking the view. Also, the side view cameras could also measure wire Z height using dual image correlation techniques. The NIR camera used in this study is spectrally bandwidth limited on the long wavelength side out to 1 micron. This limits the low temperature range sensitivity. Metals such as aluminum have a lower melting temperature and the melt pool could not be imaged using this

sensor. A sensor in the short wave infrared (SWIR) band (out to 1.7 microns) would be ideal. Also, a SWIR infrared camera would allow for more sensitivity in measuring the transient cool down and thus allow for deeper inspections. Finally for space applications, the infrared camera can be implemented onto the portable $EBF^3$ system under development [3]. The portable system will use a lower voltage electron beam, lower mass and size, and provide improved safety. $EBF^3$ welding in a zero gravity environment may allow for unique advantages in the manipulation of the weld pool during builds. Also the advantage of building parts in space provides the capability for long duration human space flights.

## REFERENCES


[1] K. M. B. Taminger et. al., "Solid freeform fabrication apparatus and methods", U. S. Patent 7,168,935, filing date Aug. 2003, issued Jan. 2007.

[2] K. M. B. Taminger and R. A. Hafley, "Electron Beam Freeform Fabrication: A Rapid Metal Deposition Process", 3rd Annual Automotive Composites Conference, Troy, MI; September 9-10, 2003.

[3] J. K. Watson, K. M. Taminger, R. A. Hafley, and D. D. Petersen, "Development of a Prototype Low-Voltage Electron Beam FreeForm Fabrication System", 13th Solid Freeform Fabrication Symposium, University of Texas at Austin, August 2007.

[4] Technical Manual Allied Vision Technologies, www.alliedvisiontec.com/.../70-0064_GC_TechMan_V2.0.pdf, April 2013.

[5] Tietjen, A. B. and Hand, D. "Calibration and Data Analysis Summary Report-HYTHIRM STS-119, STS-125 and STS-128," HYTHIRM Internal Report, Dec. 2009.

[6] Spisz, T. S., Taylor, J. C., Gibson, D. M., Kwame, O. W., Horvath, T. J., Zalameda, J. N., Tomek, D. M., Berger, Tietjen, A. B., Tack, S., and Schwartz, R. J., "Processing Near-Infrared Imagery of Hypersonic Space Shuttle Reentries," Thermosense XXXII Conference at 2010 SPIE Defense, Security, and Sensing Symposium, 5-9 April 2010, Orlando, FL, Paper 7661-17.

[7] Zalameda, J. N., Horvath, T. J., Tomek, D. M., Tietjen, A. B., Gibson, D. M., Taylor, J. C., Tack, S., Bush, B. C., Mercer, C. D., and Shea, E. J., "Application of a Near Infrared Imaging System for Thermographic Imaging of the Space Shuttle during Hypersonic Re-entry," AIAA Paper 2010-245, Jan. 2010.

[8] Melting Point of 316 Stainless Steel, http://www.goodfellow.com/E/Stainless-Steel-AISI-316.html, April 2013.

[9] Melting Poitn of Ti6-4, http://asm.matweb.com/search/SpecificMaterial.asp?bassnum=MTP641, April 2013.

[10] Emissivity of 316 Stainless Steel, http://www.coleparmer.com/TechLibraryArticle/254, April 2013.

[11] M. Boivineau, C. Cagran, D. Doytier, V. Eyraud, M-H. Nadal, B. Wilthan, and G. Pottlacher. "Thermophysical properties of solid and liquid Ti-6Al-4V (TA6V) alloy." *International journal of thermophysics* 27, no. 2 (2006): 507-529.

[12] W. J. Seufzer and K. M. Taminger, "Control of Space-Based Electron Free Form Fabrication", ADM002161, Symposium on Solid Freeform Fabrication (SFF)(18th) held in Austin, TX on 6-8 August 2007. Published in Proceedings on Solid Freeform Fabrication (SFF) (18th), pvii-ix,1-609, 2007.

[13] E. Rodriguez, F. Medina, D. Espalin, C. Terrazas, D. Muse, C. Henry, and R. B. Wicker, "Integration of a Thermal Imaging Feedback Control System in Electron Beam Melting", W. M. Keck Center for 3D Innovation, University of Texas at El Paso, August 15, 2012.

[14] K. A. Mansoor, N. H. Madsen and B. A. Chin, "Infrared Thermography as a Control for Welding Process",*Proc. SPIE* 0446, Thermosense VI: Thermal Infrared Sensing for Diagnostics and Control, 154 (March 27, 1984).

[15] Mark J Adams et al, "Method of and apparatus for thermographic evaluation of spot welds", U. S. Patent 4,854,724, filing date March 1986, issued Aug. 1989.

[16] S. M. Shepard, B. B. Chaudhry, R. L. Predmesky, and M. J. Zaluzec, "Pulsed Thermographic Inspection of Spot Welds", SPIE Proceedings Vol. 3361, Thermosense XX, John R. Snell, Jr.; Richard N. Wurzbach, Editors, pp.320-324.

[17] Cramer, K. E., and W.P. Winfree, "Method and apparatus for the portable identification of material thickness and defects using spatially controlled heat application", US Patent 6000844,(1999).

[18] J. Schlichting et. al., "Flying Laser Spot Thermography for the Fast Detection of Surface Breaking Cracks", 18th World Conference on Nondestructive Testing, 16-20 April 2012, Durban, South Africa.